Available online at www.sciencedirect.com

ScienceDirect

IFAC PapersOnline CONFERENCE PAPER ARCHIVE

IFAC PapersOnLine 55-6 (2022) 310–316

Actuator fault tolerant control via active fault diagnosis for a remotely operated vehicle

Alessandro Baldini * **Riccardo Felicetti** * **Alessandro Freddi** * **Sauro Longhi** * **Andrea Monteriù** *

* *Dipartimento di Ingegneria dell'Informazione, Università Politecnica delle Marche, Via Brecce Bianche, 60131 Ancona, Italy.*
e-mail: {a.baldini, r.felicetti, a.freddi, s.longhi, a.monteriu}@univpm.it

Abstract: Unmanned underwater vehicles operate in unstructured and harsh environments, and fault diagnosis together with fault tolerant control play a crucial role to prevent the mission from failing. When a fault occurs in presence of unknown disturbances, such as unknown marine current or hitting an obstacle, actuator fault diagnosis becomes more challenging, because the unexpected forces that arise from disturbances may be mistaken for actuator faults. In this paper, we propose an active fault diagnosis method to discern between an actuator fault and any other disturbance: the former is modelled as a multiplicative input fault, and the latter is an unknown, additive, time varying force. Once the actuator faults have been isolated and identified, their estimations are fed to the control allocation algorithm to perform fault tolerant control allocation. Simulation results are performed with a realistic non-linear model to show the effectiveness of the proposed strategy.

Keywords: Active Fault Diagnosis, Fault Tolerant Control, Remotely Operated Vehicles, Unmanned Underwater Vehicles.

1. INTRODUCTION

The increasing need for reliability in the fields of mobile robotics and autonomous vehicles poses many challenging problems, for which improved Fault Detection and Diagnosis (FDD) techniques are required. On the other hand, some advanced FDD methods apparently struggle to find practical application, as if there were a gap between theory and practice. This is the case of Active Fault Diagnosis (AFD), which has a small impact on real world problems (Punčochář and Škach, 2018) and for which researchers are still looking for new areas of application (Heirung and Mesbah, 2019). In this regard, the purpose of this paper is to show how AFD (in particular, active fault isolation) can be applied to isolate actuator faults in Remotely Operated Vehicles (ROVs) despite the presence of external disturbances, and integrated to perform fault tolerant control.

AFD mainly consists of designing an adequate auxiliary input, injecting it into the system through the input signals (e.g., adding it), and then using the input-output data for fault diagnosis. AFD overcomes the limitations of passive diagnosis in case of uncertainties, incomplete knowledge of the system, low signal-to-noise ratio, disturbances, masked fault effects by feedback control laws, and small (or slowly increasing) faults (Heirung and Mesbah, 2019).

The main concern in the AFD literature is the design of the auxiliary signal, while the input-output data is usually dealt with traditional diagnostic algorithms (i.e., the same employed in passive FDD). Common requirements to be satisfied in auxiliary signal design are: to guarantee a sufficient confidence in diagnosis, to minimize the duration of the auxiliary input (i.e., fast diagnosis), to minimize the impact on system dynamics (e.g., minimizing the magnitude of the auxiliary input), and to satisfy input and state constraints. In order to fulfil such a number of requirements, some recent AFD schemes rely on optimization methods to design the auxiliary input (Heirung and Mesbah, 2019). Several valuable works concerning AFD advances have been recently published. In Boem et al. (2019), the authors develop an active fault isolation scheme for a generic class of distributed systems, although the FDD algorithm is essentially a local one (i.e., independently performed in each subsystem). The authors of Blanchini et al. (2017) consider constant and sinusoidal auxiliary inputs only, in order to greatly simplify the online design of the auxiliary input. Also, the recent work Yang et al. (2020) provides an online two-step method to calculate the auxiliary input for model separation.

The multiple model approach is predominant in the AFD literature, but it suffers from a curse of dimensionality: when the number of possible faults increases, and also when each fault does not have a prescribed amplitude (e.g., continuous fault signal), the number of models rapidly increase as well. This issue may represent one of the main limitations in the applications, because fairly complex systems easily become intractable. Multi-parametric programming (to move part of the computation offline) and resorting to suboptimal solutions (e.g., considering only a subset of the possible models at a time) partially miti-

10.1016/j.ifacol.2022.07.147

gate the increase of complexity (Marseglia and Raimondo, 2017).

AFD has not seen widespread adoption in practical applications (Heirung and Mesbah, 2019), thus only few advances have been made in the field of mobile robots. Nevertheless, it is worth noting that most of them deal with actuator faults, that is the focus of this paper. The authors of Zhang et al. (2013) deal with a four wheel drive robot. They inject a virtual fault into the control allocation scheme in order to distinguish between front and rear wheel faults. The AFD method is borrowed from Wang and Wang (2011), where abrupt faults are taken into account. In Ducard and Geering (2008), the authors propose to inject a sinusoidal signal with an adaptive amplitude to isolate actuator faults in an Unmanned Aerial Vehicle (UAV). In Bateman et al. (2011), instead, the authors inject sinusoidal signals in the null space of the control allocation matrix, in order to isolate control surface faults in an UAV without perturbing the vehicle dynamics in the fault free case. At least two ways allow to easily inject signals in the null space: randomly weighting the control effort (Buffington et al., 1998) and randomly perturbing the actuator preferred value (Doman and Ngo, 2002). Both methods have been developed for the effectiveness matrix identification in UAVs, and they essentially consist in manipulating the cost function of an optimization-based control allocation algorithm. In this way, there is no need to calculate the null space of the effectiveness matrix. More generally, the authors of Nikoukhah and Campbell (2008) focus on incipient multiplicative faults. They point out that separability may not be guaranteed in presence of multiplicative uncertainties (i.e., no proper auxiliary input may exist).

The FDD problem in ROVs is crucial, as unmanned underwater vehicles in general face an unstructured and harsh environment where many unpredictable events may occur. The marine current can act as an external disturbance, physical obstacles may block the ROV, and aquatic vegetation can hinder the ROV's thrusters (Capocci et al., 2018). The latter, in particular, can compromise the regular functioning of the thrusters because of a partial Loss Of Effectiveness (LOE). Also note that voltage drops and propeller damaging can cause an actuator LOE as well.

In this paper, an AFD strategy is developed to discern actuator faults from any other kind of unknown disturbance. According to the classification in Punčochář and Škach (2018), the proposed method is a fixed finite time interval injection for model discrimination purposes. The auxiliary input is designed in order to have a null effect on the nominal system, because it is injected in the null space of the control effectiveness matrix. Actuator faults are modeled as a multiplicative fault, which fits well in case of actuator LOE; instead, disturbances are represented by an unknown, additive, time varying force. Once the actuator faults are actively isolated, fault identification is perfomed, and fault estimations are fed to the control allocation algorithm to perform fault tolerant control allocation.

The paper is structured as follows. In Section 2, the ROV is modeled and actuator faults are detailed. Section 3 shows the fault detection algorithm, which makes use of a Sliding Mode Observer (SMO) to add analytical redundancy. In Section 4, the AFD strategy is introduced to isolate actuator faults and, eventually, to estimate them. Simulation results using a detailed non-linear model are shown in Section 5. Finally, Section 6 concludes the paper.

2. SYSTEM MODEL

In this section, the mathematical model of an X-shaped ROV is presented at first. Then, actuator faults are introduced and modeled. Finally, the overall control scheme is reported for clarity.

2.1 ROV Dynamics

The mathematical model of the ROV in exam has been thoroughly detailed in Corradini et al. (2011). In the following, we resume the essentials. The ROV is modeled as single rigid body with six degrees of freedom. Fig. 1 shows the reference system $R-\{O,X,Y,Z\}$ is an earth fixed frame and $R_a-\{O_a,X_a,Y_a,Z_a\}$ is a body-fixed frame, whose origin coincides with the system's center of mass. The variables $[x,y,z]^T$ describe the center of mass position with respect to R, while the orientation of the vehicle is given by the conventional roll, pitch, and yaw angles (φ, θ, and ψ, respectively). The attitude dynamics is given by the angular velocities p, q, and r in R_a. Let us assume roll and pitch are stable and heave is controlled independently. The remaining surge, sway, and yaw dynamics are given by the non-linear model in (1) (on the top of the page). In particular, V_{cx} and V_{cy} are the components of the underwater current velocity in the earth fixed frame, ψ_c is the angle between the X-axis and the velocity direction of the marine current, and $p_1,\dots,p_9$ are constant parameters. Finally, $\boldsymbol{\tau}=[T_x,T_y,M_z]^T$ represents the generalized forces and moments in the earth frame R. The model (1) is more conveniently expressed in a compact form, separating the non-linear terms from the input term, as:

$$\begin{aligned}\dot{\boldsymbol{x}}_1&=\boldsymbol{x}_2\\ \dot{\boldsymbol{x}}_2&=\boldsymbol{f}(\boldsymbol{x}_1,\boldsymbol{x}_2,\hat{V}_{cx},\hat{V}_{cy},\hat{\psi}_c)+\boldsymbol{M}^{-1}\boldsymbol{\tau},\end{aligned}\tag{2}$$

where $\boldsymbol{x}_1=[x\ \ y\ \ \psi]^T$, $\boldsymbol{x}_2=[\dot{x}\ \ \dot{y}\ \ \dot{\psi}]^T$, and $\boldsymbol{M}=\mathrm{diag}(p_1,p_1,p_6)$. Please note that $\hat{V}_{cx}$, $\hat{V}_{cy}$, and $\hat{\psi}_c$ represent the marine current estimation. The possible estimation error is treated as a disturbance in the following subsection. We also assume that both $\boldsymbol{x}_1$ and $\boldsymbol{x}_2$ are available in the remainder of the paper, whether they are directly measured or properly estimated.

2.2 Control inputs and faults

The generalized forces and moments are given by:

$$\begin{aligned}\boldsymbol{\tau}&=\boldsymbol{B}(\psi)\boldsymbol{W}\boldsymbol{u}+\boldsymbol{d}=\boldsymbol{B}_\psi(\psi)\boldsymbol{B}_\alpha\boldsymbol{W}\boldsymbol{u}+\boldsymbol{d}\\&=\begin{bmatrix}c_\psi&-s_\psi&0\\ s_\psi&c_\psi&0\\0&0&1\end{bmatrix}\begin{bmatrix}c_\alpha&c_\alpha&c_\alpha&c_\alpha\\-s_\alpha&-s_\alpha&s_\alpha&s_\alpha\\-l_\alpha&l_\alpha&-l_\alpha&l_\alpha\end{bmatrix}\boldsymbol{W}\boldsymbol{u}+\boldsymbol{d},\end{aligned}\tag{3}$$

where α defines the thrusters' orientation (Fig. 2), c_α and s_α are shorts for $\cos(\alpha)$ and $\sin(\alpha)$ respectively, $l_\alpha=l_y c_\alpha+l_x s_\alpha$ is the moment arm of each thrust, l_x, l_y denote the ROV size, and $\boldsymbol{u}=[u_1,u_2,u_3,u_4]^T$ represents the forces demanded to each thruster. We also denote with $\boldsymbol{d}$ the lumped effects of external disturbances and

$$
\begin{aligned}
p_1\ddot{x} - (p_2\,|\cos(\psi)| + p_3\,|\sin(\psi)|)\,(V_{cx}-\dot{x})\sqrt{(V_{cx}-\dot{x})^2+(V_{cy}-\dot{y})^2} + p_4 x - p_5 V_{cx}\sqrt{V_{cx}^2+V_{cy}^2} &= T_x \\
p_1\ddot{y} - (p_2\,|\sin(\psi)| + p_3\,|\cos(\psi)|)\,(V_{cy}-\dot{y})\sqrt{(V_{cx}-\dot{x})^2+(V_{cy}-\dot{y})^2} + p_4 y - p_5 V_{cy}\sqrt{V_{cx}^2+V_{cy}^2} &= T_y \\
p_6\ddot{\psi} + p_7\dot{\psi}\left|\dot{\psi}\right| + p_8(V_{cx}^2+V_{cy}^2)\sin\left(\frac{\psi-\psi_c}{2}\right) + p_9 &= M_z
\end{aligned}
\tag{1}
$$

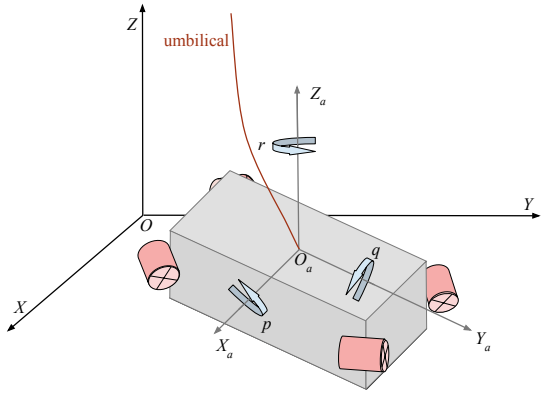

Fig. 1. Earth fixed inertial frame $R-\{O,X,Y,Z\}$ and body frame $R_a-\{O_a,X_a,Y_a,Z_a\}$.

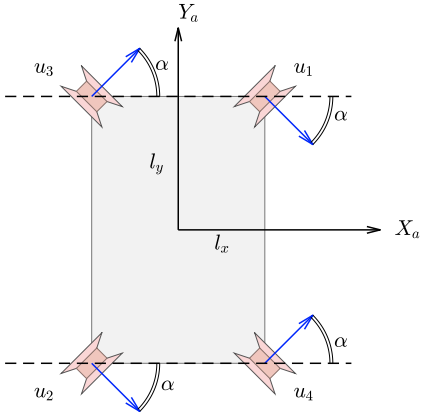

Fig. 2. Thruster configuration. The blue arrows point in the positive thrust direction.

model uncertainties, e.g., mismatch between the actual marine current and its estimation. We define $\boldsymbol{B}(\psi)\boldsymbol{W}$ as the control effectiveness matrix (Johansen and Fossen, 2013), where $\boldsymbol{W}=\text{diag}(w_1,w_2,w_3,w_4)\in\mathbb{R}^{4\times4}$ is a diagonal time-varying matrix that models the actuators' health. In absence of actuator faults, $\boldsymbol{W}$ corresponds to the identity matrix. In general, we have

$$
\begin{aligned}
w_i = 1 \quad & \text{if the } i\text{-th actuator is healthy,} \\
w_i \in (0,1) \quad & \text{if the } i\text{-th actuator suffers LOE,} \\
w_i = 0 \quad & \text{if the } i\text{-th actuator has failed.}
\end{aligned}
$$

When $w_i<1$, the actual thrust of the i-th actuator is lower than expected (e.g., LOE as a consequence of damaged or entangled propeller (Capocci et al., 2018)), and $1-w_i$ represents the LOE magnitude. If input constraints are neglected, trajectory tracking is possible with up to 1 failure (and any number of faults), as discussed in Baldini et al. (2018b). However, faults affect the attainable control set and reduce the vehicle maneuverability. Throughout this paper, we assume actuator faults never to degenerate into failures, hence $w_i>0$ for $i=1,...,4$.

2.3 Control scheme

The overall control scheme is depicted in Fig. 3. Let $\hat{\boldsymbol{W}}=\text{diag}(\hat{w}_1,\hat{w}_2,\hat{w}_3,\hat{w}_4)$ be a piecewise constant estimation of the unknown matrix $\boldsymbol{W}$. Without loss of generality, we suppose the ROV is fully working at the beginning of a mission, so the initial value of $\hat{\boldsymbol{W}}$ is the identity matrix. Then, the fault estimation $\hat{\boldsymbol{W}}$ is updated only when a new actuator fault is isolated.

The control law provides the desired forces and moments $\boldsymbol{\tau}_c$ for tracking purposes. Thus, a control allocation algorithm calculates

$$
\boldsymbol{u}_c : \boldsymbol{\tau}_c = \boldsymbol{B}(\psi)\hat{\boldsymbol{W}}\boldsymbol{u}_c. \tag{4}
$$

We also set

$$
\boldsymbol{u} = \boldsymbol{u}_c + \boldsymbol{u}_{aux}, \tag{5}
$$

where $\boldsymbol{u}$ is the force that is demanded to the actuators, $\boldsymbol{u}_c$ is the control allocation output, and $\boldsymbol{u}_{aux}$ is an auxiliary input to perform AFD. The proposed scheme employs a fixed finite time interval injection: we have $\boldsymbol{u}_{aux}\neq0$ only when AFD is triggered, otherwise $\boldsymbol{u}_{aux}=0$ holds during regular functioning.

3. FAULT DETECTION

In case of a wrong fault estimation ($\hat{\boldsymbol{W}}\neq\boldsymbol{W}$) or external disturbance ($\|\boldsymbol{d}\|_2>0$) we have $\boldsymbol{\tau}\neq\boldsymbol{\tau}_c$ according to (3) and (4). The following SMO is designed to estimate $\boldsymbol{\tau}-\boldsymbol{\tau}_c$. The overall ROV model (1) can be rewritten in form (2), where $\boldsymbol{\tau}$ is defined in (3). Because $\|\boldsymbol{u}\|_2$ is bounded (saturation of the real actuators), and assuming that $\|\boldsymbol{d}\|_2$ is bounded as well (finite energy disturbance), there exists ρ such that $\|\boldsymbol{M}^{-1}(\boldsymbol{\tau}-\boldsymbol{\tau}_c)\|_2\leq\rho$. The sliding mode observer is structured as follows:

$$
\begin{aligned}
\dot{\hat{\boldsymbol{x}}}_1 &= \hat{\boldsymbol{x}}_2 \\
\dot{\hat{\boldsymbol{x}}}_2 &= \boldsymbol{f}(\boldsymbol{x}_1,\boldsymbol{x}_2,\hat{V}_{cx},\hat{V}_{cy},\hat{\psi}_c) + \boldsymbol{M}^{-1}\boldsymbol{\tau}_c + \boldsymbol{\xi},
\end{aligned}
\tag{6}
$$

where $\hat{\boldsymbol{x}}_1$ and $\hat{\boldsymbol{x}}_2$ are the observer state variables and $\boldsymbol{\xi}$ is the injection term. We choose the sliding surface $\boldsymbol{s}=\boldsymbol{e}_2+\boldsymbol{K}\boldsymbol{e}_1$, where $\boldsymbol{e}_1=\boldsymbol{x}_1-\hat{\boldsymbol{x}}_1$, $\boldsymbol{e}_2=\boldsymbol{x}_2-\hat{\boldsymbol{x}}_2$, $\boldsymbol{K}=\text{diag}(k_1,k_3,k_5)$, with $k_1,k_3,k_5>0$. Let $\boldsymbol{\xi}$ be:

$$
\boldsymbol{\xi} = \boldsymbol{K}\boldsymbol{e}_2 + \boldsymbol{\Gamma}\frac{\boldsymbol{s}}{\|\boldsymbol{s}\|_2}, \tag{7}
$$

where $\boldsymbol{\Gamma}=\text{diag}(\rho+\gamma_1,\rho+\gamma_3,\rho+\gamma_5)$ and $\gamma_1,\gamma_3,\gamma_5>0$. Taking the Lyapunov candidate function $V=\boldsymbol{s}^T\boldsymbol{s}/2$, we can show that $\dot{V}\leq-\gamma\|\boldsymbol{s}\|_2$, $\gamma>0$, i.e., the observation error vanishes in finite time. Also,

$$
\boldsymbol{\xi}_{eq} = \boldsymbol{M}^{-1}(\boldsymbol{\tau}-\boldsymbol{\tau}_c) \tag{8}
$$

holds, where $\boldsymbol{\xi}_{eq}$ is the equivalent injection term (Shtessel et al. (2014)). The proof is similar to Baldini et al. (2018b) and thus omitted for brevity. We calculate $\boldsymbol{\xi}_{eq}$ online as

$$
\text{LPF}\left(\boldsymbol{\Gamma}\frac{\boldsymbol{s}}{\|\boldsymbol{s}\|_2}\right) \approx \boldsymbol{\xi}_{eq}, \tag{9}
$$

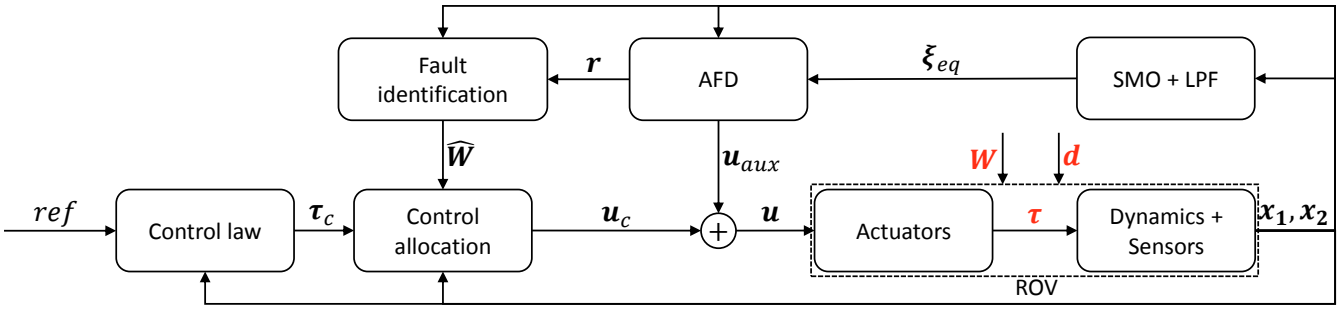

Fig. 3. Overall fault tolerant control scheme. The quantities in red cannot be measured directly.

where LPF$(\cdot)$ denotes the low pass filtering of each component.

We take $\boldsymbol{\xi}_{eq}$ as the diagnostic residual. The residual $\boldsymbol{\xi}_{eq}$ is compared with an adaptive threshold to perform fault detection. If

$$\|\Xi\boldsymbol{\xi}_{eq}\|_2 > c_1 + c_2\|\boldsymbol{\tau}_c\|_2 \tag{10}$$

holds, a fault is detected; $c_1, c_2 > 0$ are constants and Ξ is a suitable diagonal positive definite scaling matrix.

4. FAULT ISOLATION AND IDENTIFICATION

If (10) is satisfied, the reference is frozen and the ROV is stabilized in the current position through $\boldsymbol{u}_c$. Then, AFD is performed to discern between the presence of a disturbance or a new actuator fault. AFD becomes necessary because both $\boldsymbol{d}$ and $\boldsymbol{W}$ may be rewritten as a matched disturbance in the open loop system (2)–(3), and both act in the same input channels. Thus, any isolation approach must consider the fault behaviour in time to discriminate between a disturbance $\boldsymbol{d}$ and an actuator fault $\boldsymbol{W}$ successfully. As actuator faults are usually irreversible (i.e., broken or entangled propeller), we consider abrupt faults only.

4.1 Auxiliary input design

The following auxiliary signal is employed for a fixed injection time Δt:

$$\begin{aligned}\boldsymbol{u}_{aux} &= a\boldsymbol{n}_{aux}\sin(2\pi f\bar{t})\\ \boldsymbol{n}_{aux} &= \hat{\boldsymbol{W}}^{-1}[1\ -1\ -1\ 1]^T\end{aligned} \tag{11}$$

where a is the signal nominal amplitude, $\boldsymbol{n}_{aux}$ is a basis vector for the (one-dimensional) null space of $\boldsymbol{B}(\psi)\hat{\boldsymbol{W}}$, f is the signal frequency, and $\bar{t}$ is a timer running from 0 s to Δt during the AFD phase and zero otherwise. Please note that $\boldsymbol{n}_{aux} \in \mathbb{R}^{4\times 1}$ thanks to the assumption $w_i > 0$ for $i = 1, ..., 4$.

The auxiliary input (11) is chosen because it represents a null space injection. In fact, according to (3) and (5), the actual forces and moments acting on the ROV are

$$\begin{aligned}\boldsymbol{\tau} &= \boldsymbol{B}(\psi)\boldsymbol{W}(\boldsymbol{u}_c + \boldsymbol{u}_{aux}) + \boldsymbol{d}\\ &= \boldsymbol{B}(\psi)\boldsymbol{W}\boldsymbol{u}_c + a\boldsymbol{B}(\psi)\boldsymbol{W}\boldsymbol{n}_{aux}\sin(2\pi f\bar{t}) + \boldsymbol{d}.\end{aligned} \tag{12}$$

Let us assume that the current actuator fault estimation is correct ($\hat{\boldsymbol{W}} = \boldsymbol{W}$). Please note that this holds at the beginning of the mission, assuming that no actuator faults occur ($\hat{\boldsymbol{W}} = \boldsymbol{W} = \boldsymbol{I}_4$). We have $\|\boldsymbol{B}(\psi)\boldsymbol{W}\boldsymbol{n}_{aux}\|_2 = \|\boldsymbol{B}(\psi)\hat{\boldsymbol{W}}\boldsymbol{n}_{aux}\|_2 = 0$ because $\boldsymbol{n}_{aux} \in \text{null}(\boldsymbol{B}(\psi)\hat{\boldsymbol{W}})$. So,

$$\boldsymbol{\tau} = \boldsymbol{B}(\psi)\boldsymbol{W}\boldsymbol{u}_c + \boldsymbol{d}, \tag{13}$$

i.e., the auxiliary input $\boldsymbol{u}_{aux}$ has no effect on the generalized forces and moments $\boldsymbol{\tau}$ if the actuator fault estimation is correct. This means that $\boldsymbol{u}_{aux}$ has a minimal impact on the system dynamics.

On the contrary, when a fault occurs and the fault estimation is incorrect, the larger the difference $\boldsymbol{W} - \hat{\boldsymbol{W}}$, the larger the undesired force. In fact,

$$\begin{aligned}\boldsymbol{\tau} &= \boldsymbol{B}(\psi)\boldsymbol{W}(\boldsymbol{u}_c + \boldsymbol{u}_{aux}) + \boldsymbol{d}\\ &= \boldsymbol{B}(\psi)\boldsymbol{W}\boldsymbol{u}_c + a\boldsymbol{B}(\psi)(\boldsymbol{W} - \hat{\boldsymbol{W}})\boldsymbol{n}_{aux}\sin(2\pi f\bar{t}) + \boldsymbol{d}\\ &\quad + a\boldsymbol{B}(\psi)\hat{\boldsymbol{W}}\boldsymbol{n}_{aux}\sin(2\pi f\bar{t})\\ &= \boldsymbol{B}(\psi)\boldsymbol{W}\boldsymbol{u}_c + \boldsymbol{d} + \boldsymbol{B}(\psi)(\boldsymbol{W} - \hat{\boldsymbol{W}})\boldsymbol{u}_{aux},\end{aligned} \tag{14}$$

where, as in the previous case, $\|\boldsymbol{B}(\psi)\hat{\boldsymbol{W}}\boldsymbol{n}_{aux}\|_2 = 0$ has been exploited. Please note that the actual effect of $\boldsymbol{u}_{aux}$ on $\boldsymbol{\tau}$ is upper bounded by $2a\|\hat{\boldsymbol{W}}^{-1}\|_2\|\boldsymbol{B}(\psi)\|_2\|\boldsymbol{W} - \hat{\boldsymbol{W}}\|_2$, that is the worst case 2-norm of the last addend in (14). This contribution is undesired for control purposes, but it is exploited for fault isolation.

4.2 Active fault isolation

When an actuator fault occurs, the vector of sinusoidal signals $\boldsymbol{u}_{aux}$ propagates into the control system through the term $\boldsymbol{B}(\psi)(\boldsymbol{W} - \hat{\boldsymbol{W}})\boldsymbol{u}_{aux}$ in (14). On the contrary, if (10) is triggered by an external disturbance, $\boldsymbol{u}_{aux}$ does not propagate because it lies in the null space of the control effectiveness matrix, as shown in (13). The idea is to check if such sinusoidal signals of known frequency can be detected by means of a signal-based method.

In case of actuator faults, $\boldsymbol{\tau}$ clearly contains the effects of $\boldsymbol{u}_{aux}$, but $\boldsymbol{\tau}$ is not available. Also, using the SMO estimation $\boldsymbol{\xi}_{eq}$ in (9) for isolation is not practical: although f lies in the passband of the low pass filter in (9), $\boldsymbol{\xi}_{eq}$ is too noisy due to chattering. The proposed solution is to perform a spectral analysis on the measured velocities (both linear and angular ones).

Please note $\boldsymbol{u}_{aux}$ is a vector of sine functions with rectangular windowing (also see Fig. 4). Hence, spectral leakage occurs, and the main lobe of $\boldsymbol{u}_{aux}$ lies in $f \pm 1/\Delta t$. The energy in such band determines whether an actuator fault occurred or not.

We define the residual for active fault isolation $\boldsymbol{r}$ as the Discrete Fourier Transform (DFT) at the frequency f for the measured ROV velocities. If $\boldsymbol{r}$ overcomes a fixed threshold, i.e.,

$$\|\boldsymbol{R}\boldsymbol{r}\|_\infty > c_3, \tag{15}$$

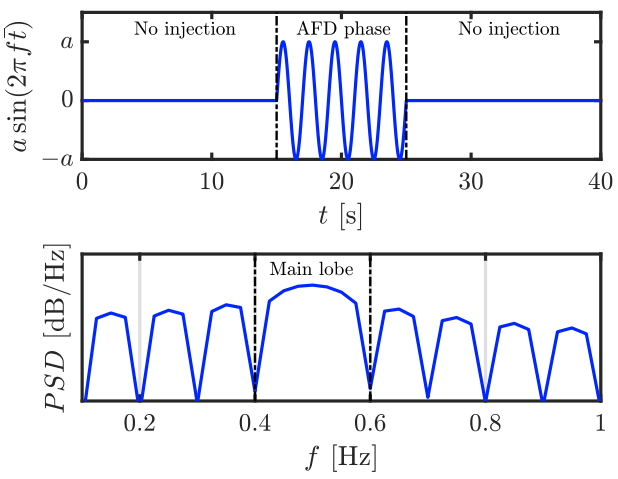

Fig. 4. AFD with fixed finite time interval injection: signal and its power spectral density ($\Delta t = 10$ s, $f = 0.5$ Hz).

where $c_3 > 0$ is a constant and $\boldsymbol{R}$ is a suitable diagonal positive definite scaling matrix, we decide the detected mismatch $\boldsymbol{\xi}_{eq}$ depends on actuator faults, and we move to the fault identification phase. Otherwise, we suppose the mismatch to be related to the unknown disturbance $\boldsymbol{d}$ because it does not fit with the multiplicative actuator fault model.

4.3 Fault identification

Two cases can occur, depending on the outcome of (15). If an unknown disturbance is acting, we take no further steps, as we have no information about $\boldsymbol{d}$ and its dynamics: the AFD phase terminates and the ROV resumes its task. In case of actuator faults, instead, we suppose LOE lasts in time. Thus, actuator fault identification is performed and $\hat{\boldsymbol{W}}$ is updated consequently, so that the control allocation algorithm can compensate such faults.

The fault identification algorithm is omitted for brevity. In the remainder, we employ a computationally cheap method that has been shown in the previous work Baldini et al. (2018c). Such algorithm is effective only under the assumption that the probability of having a disturbance and an actuator fault at the same time is negligible.

5. SIMULATION SETUP AND RESULTS

Simulation results are obtained by implementing and running the realistic non-linear model in (1) in Simulink.

5.1 Setup

Sensor noise is included and it is comparable to a low cost MPU-9250 IMU operating at 200Hz. Also, thruster dynamics are approximated by first order stable systems to improve model fidelity. The nominal marine current velocity ($V_{cx} = V_{cy} = 0.2$m/s) is available to the control law. A backstepping controller (detailed in Baldini et al. (2018a)) is employed, while the control allocation is dealt with an active-set QP solver. In the simulation, the ROV tracks a counter-clockwise elliptic trajectory (Fig. 5) and it is subject to the following conditions:

C1) an unknown external disturbance, in $t \in [30, 60]$ s, given by an unmeasured marine current variation ($V_{cx} = 0.3$ m/s, $V_{cy} = 0.1$ m/s);
C2) a fault on actuator 3, at $t = 70$ s, with $w_3 = 0.7$;
C3) a fault on actuator 2, at $t = 110$ s, with $w_2 = 0.4$;

The low pass filter as of (9) is designed in Simulink using the Digital Filter Design tool. A minimum order IIR Butterworth filter is employed to get both acceptable chattering attenuation and sufficiently short response time. The specifications are: 200 Hz sampling, 0.5 Hz passband frequency (maximum attenuation 0.05 dB), 5 Hz stopband frequency with 140 dB attenuation. The resulting filter order is 8.

Please note that low sampling rate is a common issue in commercially available ROVs. If the sampling frequency is lower than 200Hz, adding cheap high rate sensors and performing multi rate sensor fusion, as done in Bandala et al. (2014), may represent a practical solution.

Given a 200 Hz sampling, we take the last 4 s of the velocity signals during the AFD injection, such that the frequency resolution of DFT is 0.25 Hz and we can calculate the DFT at 0.5 Hz. In order to avoid performing FFT online, we employ the Goertzel algorithm to evaluate the DFT at a single frequency.

5.2 Results

The fault estimation, provided by the SMO, is shown in Fig. 6. The dash-dotted vertical lines represent the beginning of an AFD phase. Each one is triggered by the condition (10): Fig. 6 reports the residual norm and the adaptive threshold. Choosing $\boldsymbol{\Xi} = \boldsymbol{M}$ (see Table 1 for the full list of parameters), we have $\boldsymbol{\Xi}\boldsymbol{\xi}_{eq} \approx \boldsymbol{\tau} - \boldsymbol{\tau}_c$ according to (8). The equality is not strict for several reasons: low pass filter distortion and delay, unmodeled actuator dynamics, sensor noise, etc.

Table 1. Adopted parameters.

Parameter	$\boldsymbol{\Xi}$	c_1	c_2	c_3	$\boldsymbol{R}$	a	f
Value	$\boldsymbol{M}$	300	1/15	1/1000	$\boldsymbol{I}_3$	500	0.5

The DFT at $f = 0.5$ Hz of each measured velocity, during the last 4 s of AFD, is reported in Table 2. In absence of actuator faults, none of the residuals overcome the threshold. On the contrary, at least one residual is large enough to isolate the actuator fault.

The control input $\boldsymbol{u}$ is shown in Fig. 7. As soon as the AFD phase begins, the sinusoidal $\boldsymbol{u}_{aux}$ is injected for 10 s. The input ripples, that occur after each dash-dotted vertical line in Fig. 7, are due to $\boldsymbol{u}_{aux}$.

The actual references, including three stops due to FDD, are shown in Fig. 8. In addition, Fig. 9 shows the trajectory error, where small ripples can be noticed during the AFD injection in presence of actuator faults. Please note the control system is inherently robust to the external disturbance, even if no information is provided. On the contrary, if actuator faults are not estimated and actively compensated by the control allocation algorithm, the tracking performances deteriorate significantly, as shown in the previous work Baldini et al. (2018a). Finally, the actuator

fault estimation is shown in Fig. 10: healthy actuators are omitted for brevity.

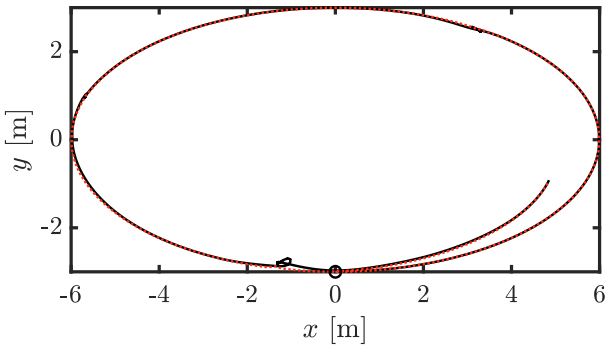

Fig. 5. Reference trajectory (red dotted line) and ROV position (black solid line). The initial position is denoted by a black circle.

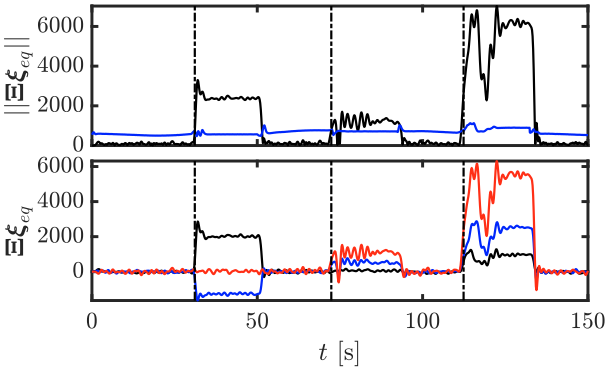

Fig. 6. Detection residual norm (in black) and adaptive threshold (in blue); fault detection and identification (T_x in black, T_y in blue, M_z in red);

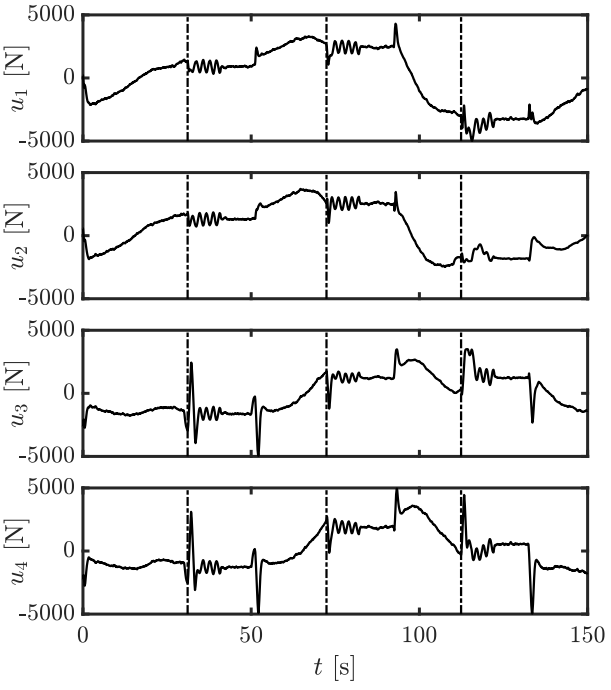

Fig. 7. Control inputs.

Table 2. DFT of $\boldsymbol{r}$ at 0.5 Hz. The underlined quantities overcome the threshold c_3 ($\boldsymbol{R} = \boldsymbol{I}_3$).

	r_1	r_2	r_3
C1)	6.9215e-5	2.2834e-4	4.9884e-5
C2)	3.4779e-4	2.0921e-3	2.8153e-3
C3)	3.2926e-3	6.6291e-3	1.0899e-2

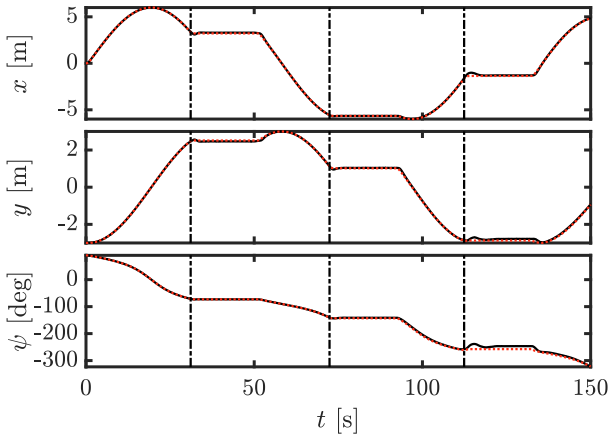

Fig. 8. Actual reference (red dotted line) and ROV state (black solid line).

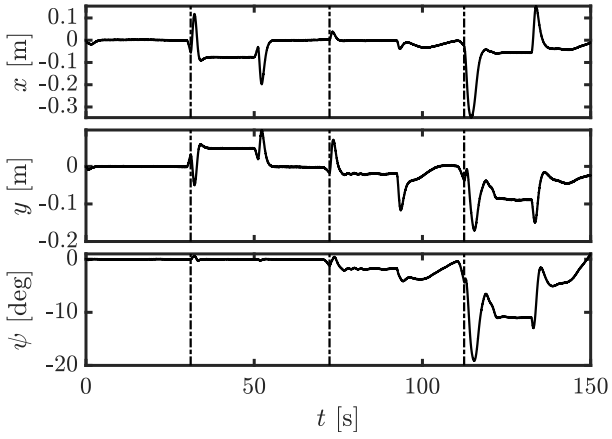

Fig. 9. Tracking errors.

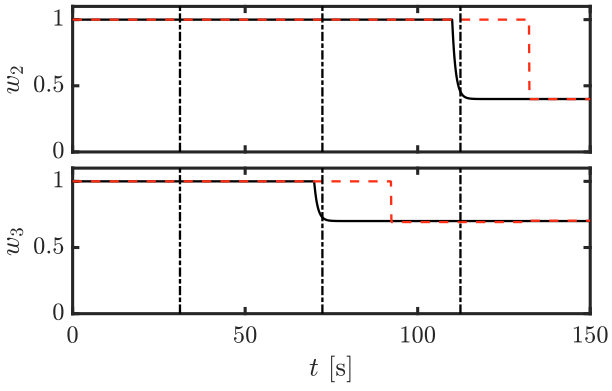

Fig. 10. Actuator faults (black solid line) and their estimation (red dashed line).

6. CONCLUSIONS

In this paper, an AFD strategy has been developed for actuator faults in a ROV. The impact of the auxiliary input $\boldsymbol{u}_{aux}$ on the closed loop system has been minimized in two ways, i.e., by setting $\boldsymbol{u}_{aux} = 0$ when no faults are detected and by injecting the auxiliary input in the null space of the control effectiveness matrix when faults are detected. If no actuator fault occurs, the injection of $\boldsymbol{u}_{aux} \neq 0$ has no effect on the system. Otherwise, the measured variables show a small ripple, that can be detected in the frequency domain. The simulations have shown that the method can discern between actuator faults and external disturbances, provided that a sufficiently high sensor sampling rate is available. Also note the Goertzel algorithm represents a computationally efficient method to calculate the DFT for a single frequency, thus it can be implemented online.

REFERENCES

Baldini, A., Ciabattoni, L., Felicetti, R., Ferracuti, F., Freddi, A., and Monteriù, A. (2018a). Dynamic surface fault tolerant control for underwater remotely operated vehicles. *ISA Transactions*, 78, 10–20.

Baldini, A., Fasano, A., Felicetti, R., Freddi, A., Longhi, S., and Monteriù, A. (2018b). A model-based active fault tolerant control scheme for a remotely operated vehicle. *IFAC-PapersOnLine*, 51(24), 798–805.

Baldini, A., Felicetti, R., Freddi, A., Longhi, S., Monteriù, A., and Fasano, A. (2018c). Fault detection, diagnosis and fault tolerant output control for a remotely operated vehicle. In *2018 14th IEEE/ASME International Conference on Mechatronic and Embedded Systems and Applications (MESA)*, 1–7. IEEE.

Bandala, M., Salgado, T., and Chávez, R. (2014). Multirate sensor fusion for underwater heading estimation. *Industrial Robot: An International Journal*.

Bateman, F., Noura, H., and Ouladsine, M. (2011). Fault diagnosis and fault-tolerant control strategy for the aerosonde uav. *IEEE Transactions on Aerospace and Electronic Systems*, 47(3), 2119–2137.

Blanchini, F., Casagrande, D., Giordano, G., Miani, S., Olaru, S., and Reppa, V. (2017). Active fault isolation: A duality-based approach via convex programming. *SIAM Journal on Control and Optimization*, 55(3), 1619–1640.

Boem, F., Gallo, A.J., Raimondo, D.M., and Parisini, T. (2019). Distributed fault-tolerant control of large-scale systems: an active fault diagnosis approach. *IEEE Transactions on Control of Network Systems*, 7(1), 288–301.

Buffington, J., Chandler, P., and Pachter, M. (1998). Integration of on-line system identification and optimization-based control allocation. In *Guidance, Navigation, and Control Conference and Exhibit*, 4487.

Capocci, R., Omerdic, E., Dooly, G., and Toal, D. (2018). Fault-tolerant control for rovs using control reallocation and power isolation. *Journal of Marine Science and Engineering*, 6(2), 40.

Corradini, M.L., Monteriù, A., and Orlando, G. (2011). An actuator failure tolerant control scheme for an underwater remotely operated vehicle. *IEEE Transactions on Control System Technology*, 19(5), 1036–1046.

Doman, D.B. and Ngo, A.D. (2002). Dynamic inversion-based adaptive/reconfigurable control of the x-33 on ascent. *Journal of Guidance, Control, and Dynamics*, 25(2), 275–284.

Ducard, G. and Geering, H.P. (2008). Efficient nonlinear actuator fault detection and isolation system for unmanned aerial vehicles. *Journal of Guidance, Control, and Dynamics*, 31(1), 225–237.

Heirung, T.A.N. and Mesbah, A. (2019). Input design for active fault diagnosis. *Annual Reviews in Control*, 47, 35–50.

Johansen, T.A. and Fossen, T.I. (2013). Control allocation - a survey. *Automatica*, 49(5), 1087–1103.

Marseglia, G.R. and Raimondo, D.M. (2017). Active fault diagnosis: A multi-parametric approach. *Automatica*, 79, 223–230.

Nikoukhah, R. and Campbell, S.L. (2008). On the detection of small parameter variations in linear uncertain systems. *European Journal of Control*, 14(2), 158–171.

Punčochář, I. and Škach, J. (2018). A survey of active fault diagnosis methods. *IFAC-PapersOnLine*, 51(24), 1091–1098.

Shtessel, Y., Edwards, C., Fridman, L., and Levant, A. (2014). *Sliding mode control and observation*, volume 10. Springer.

Wang, R. and Wang, J. (2011). Fault-tolerant control with active fault diagnosis for four-wheel independently driven electric ground vehicles. *IEEE Transactions on Vehicular Technology*, 60(9), 4276–4287.

Yang, S., Xu, F., Wang, X., and Liang, B. (2020). A novel online active fault diagnosis method based on invariant sets. *IEEE Control Systems Letters*, 5(2), 457–462.

Zhang, X., Cocquempot, V., Jiang, B., and Yang, H. (2013). Active fault diagnosis based on fault-tolerant control with control constraints for an electric 4wd vehicle. In *2013 10th IEEE International Conference on Control and Automation (ICCA)*, 1724–1729. IEEE.